

Approximate Dynamics Lead to Optimal Control: Efficient Calculation of Exact Derivatives

Jesper Hasseriis Mohr Jensen¹, Frederik Skovbo Møller^{1,2}, Jens Jakob Sørensen¹, and Jacob Friis Sherson^{1*}

¹ *Department of Physics and Astronomy, Aarhus University,
Ny Munkegade 120, 8000 Aarhus C, Denmark and*

² *Vienna Center for Quantum Science and Technology,
Atominstitut, TU Wien, Stadionallee 2, 1020 Vienna, Austria*

We discuss the importance of accurate derivatives for efficiently locally traversing and converging in optimization landscapes. In the context of quantum optimal control, we find that the feasibility of meeting this central requirement critically depends on the choice of propagation scheme and problem representation by deriving analytically exact control derivatives (gradient and Hessian). Even when exact propagation is sufficiently cheap, we find, perhaps surprisingly, that it is always much more efficient to optimize the (appropriately) approximate propagators: in a certain sense, approximations in the dynamics is traded off for significant complexity reductions in the exact derivative calculations. We quantitatively verify these claims for two concrete problems of increasing Hilbert space dimensionality and find that the best schemes obtain unit fidelity to machine precision, whereas the results for other schemes are separated consistently by orders of magnitude in computation time and in worst case 10 orders of magnitude in achievable fidelity. Since these gaps will continually increase with system size and complexity, this methodology unlocks efficient optimization of many-body dynamics operating in the unprecedented high-fidelity regime which will be published separately.

I. INTRODUCTION

The demand for precise quantum control extending into high-fidelity regimes places increasing emphasis on the role of optimization methodologies and their performance capacities. Identification and extraction of quantum *optimal controls* has enjoyed theoretical and experimental success in numerous research areas [1], such as superconducting qubits [2–6], nuclear magnetic resonance systems [7–11], nitrogen vacancy centers [12–15], cold molecules [16–19], and cold atoms [20–25], to name a few. At the same time, an increasing array of algorithmic approaches are available in these arenas, counting among others derivative-based (GRAPE [8, 26, 27], GOAT [28], GROUP [11, 29], Krotov [30–32]), derivative-free (Nelder-Mead CRAB [20, 21, 33], stochastic ascent [34], genetic evolutionary [35]), and combinations thereof [36]. Along a separate axis lies additional choices of open-loop [37, 38], closed-loop [39–41], and/or human-in-the-loop [42, 43] control.

Regardless of particulars pertaining to the physical platforms and angles of attack for the optimization itself, a shared common denominator is inevitable: in tandem with growing problem complexity and numerical simulation efforts, the relative efficiency of each optimization cycle must be maximized to allow convergence to high-fidelity solutions within finite time. Accuracy and computational speed have been identified as important goals and challenges for modern control design [1, 44], and in the context of gradient-based methods, this has been recognized at least since a seminal work Ref. [8] where the analytical first-order approximation to the gradient was

calculated. This first-order approximation, however, is not suited for obtaining standard quasi-Newton search directions due to the rapid error accumulation in the Hessian approximation, which is built iteratively from gradients [45]. The steepest descent direction is also only a minimally viable choice with the weakest convergence properties. The use of quasi-Newton methods with the more desirable convergence properties was enabled later in Ref. [26] where the analytically exact gradient for an exact propagator was calculated at the expense of additional computational time per iteration. As system sizes increase, however, exact propagators become infeasible.

In this work, we hope to advance the theoretical toolbox for obtaining high-fidelity state transfer controls in a formalistically general setting by deriving *analytically exact* gradients as well as Hessians for different propagation schemes, specifically the exact propagator and two second-order Suzuki-Trotter propagators, which we interpret in terms of optimization landscapes. This means that each choice of effective time evolution operator gives rise to its own (not necessarily exact) optimization landscape. Apart from the (sometimes computationally infeasible) exact approach, we thus examine the interplay between approximations in the landscape versus in the derivative calculations. We note that only the exact gradient derivation for the exact propagator is similar to the calculations in Ref. [26]. Another state-of-the-art approach to calculating both derivatives is through the so-called *auxiliary matrix method* [46, 47] as implemented e.g. in the Spinach software library [48], and we include this methodology in our comparative studies.

We show that the complexity of exact analytical derivatives strongly depend on the chosen scheme (corresponding to numerical implementation details) and representation of the problem: solving the problem in a basis where the controllable part of the Hamiltonian is diago-

* sherson@phys.au.dk

nal and simultaneously employing one of the Trotterized propagators greatly simplifies the derivative calculations. Especially, the exact gradient for the exact landscape entails an expensive (i) infinite recursive commutator summation in powers of the time step where the first term corresponds to a first-order approximation, or (ii) matrix exponential. On the other hand, the infinite series terminates identically for the Trotterized landscapes and only the first-order term is needed to be analytically exact. Thus, with those considerations, *analytically exact* gradients can be computed very efficiently, principally limited only by the time it takes to propagate states. To cement these findings and novel calculations, we first consider a two-level Landau-Zener (LZ) problem and indeed find that optimizing in the Trotterized landscapes rapidly yields optimal results to machine precision for that problem. Optimizing in the exact landscape is also feasible if using exact derivatives, where solutions of the same quality are obtained but is an order of magnitude slower per iteration. Using instead the first-order approximation to the derivatives consistently yields 10 orders of magnitude worse results, while also being slower per iteration. The demonstration shows that, even in a minimal problem, optimizing in the Trotterized landscapes with appropriate exact derivatives is hugely beneficial. We then consider another problem for optimization, a nine-level transmon system, and find the same performance hierarchy, except the feasibility gap to the exact landscapes have greatly increased (this trend is monotonic in the face of more complex and larger systems). As the Hilbert space dimension scales exponentially in the number of constituent, this becomes especially relevant when the system size enters the many-body regime, where exact diagonalization, exact propagation, and infinite summation or auxiliary matrix exponentiation of the associated exact derivatives are completely outside numerical feasibility.

II. EXACT DERIVATIVES FOR QUANTUM OPTIMAL CONTROL

In quantum optimal control we seek to steer some quantum mechanical process in a controlled way such as to maximize a desired physical yield. The manipulatory access to the system dynamics is through one or more control parameters in the Hamiltonian, $\hat{H} = \hat{H}(u(t))$. A broad class of control problems deal with maximizing a *state transfer*, $|\psi_{\text{ini}}\rangle \rightarrow |\psi_{\text{tgt}}\rangle$, ideally to near unit fidelity or equivalently zero cost, given respectively by

$$F = |\langle \psi_{\text{tgt}} | \psi(T) \rangle|^2 = |\langle \psi_{\text{tgt}} | \hat{U}(T; 0) | \psi_{\text{ini}} \rangle|^2, \quad (1)$$

$$J_F = \frac{1}{2} (1 - F), \quad (2)$$

where $|\psi_{\text{tgt}}\rangle$ is the target state, $|\psi_{\text{ini}}\rangle$ is the initial state, $|\psi(T)\rangle = \hat{U}(T; 0) |\psi_{\text{ini}}\rangle$ is the time evolved state at final time T with $\hat{U}(T; 0)$ being the time evolution operator

from $t = 0 \rightarrow T$. Since a *gate synthesis* problem (e.g. a CNOT gate) is equivalent to a number of simultaneous state transfers, corresponding to the mappings defined by the gate, we restrict our attention to the state transfer formulation in this paper.

For numerical (and as we shall see, analytical) convenience it is natural to discretize time in regular δt intervals, leading to piece-wise constant time evolution operators

$$t \in [t_1, t_2, \dots, t_{N_t}] = [0, \delta t, \dots, T], \quad (3)$$

$$\hat{U}(T; 0) = \prod_{j=1}^{N_t-1} \hat{U}_j = \hat{U}_{N_t-1} \dots \hat{U}_2 \hat{U}_1, \quad (4)$$

where each $\hat{U}_n = \hat{U}(u_n) = \exp(-i\hat{H}(u_n)\delta t)$ with $u_n = u(t_n)$ evolves the state as $|\psi_{n+1}\rangle = \hat{U}_n |\psi_n\rangle$ and $|\psi_1\rangle = |\psi_{\text{ini}}\rangle$. We assume $\hat{H}_n = \hat{H}(u_n) = \hat{H}_n^d + \hat{H}_n^c$ where $\hat{H}_n^c = \hat{H}(t_n, u_n)$ and $\hat{H}_n^d(t_n)$ are the control and drift Hamiltonians, respectively, both generally allowed to be time-dependent. Inclusion of M control Hamiltonians $\hat{H}_n^c \rightarrow \sum_{m=1}^M \hat{H}_{n,m}^c(u_{n,m})$ is straightforward [49], and we take $M = 1$ to preserve clarity of the presentation.

The task thus consists in finding appropriate control vector(s) $\vec{u} = (u_1, \dots, u_{N_t})^T$ that minimizes (2) corresponding to local (hopefully global) minima in the control landscape defined by $J_F = J_F(\vec{u})$. There are a plethora of techniques and ideas to maneuver the landscape in search of such minima. In this paper we focus on derivative-based local optimization methodologies, characterized by making informed decisions in traversing the control landscape $\vec{u}^{(k)} \rightarrow \vec{u}^{(k+1)}$ using local information at iteration k about the landscape topography. Concretely, in prototypical linesearch-based updates on the form

$$\vec{u}^{(k+1)} = \vec{u}^{(k)} + \alpha^{(k)} \vec{p}^{(k)}, \quad \alpha^{(k)} \in \mathbb{R}^+, \quad (5)$$

the search direction $\vec{p}^{(k)}$ is calculated from the current local gradient (e.g. steepest descent, conjugate gradient, quasi-Newton directions) and possibly also the Hessian (e.g. Newton direction), whereas the step size $\alpha^{(k)}$ is determined by an inexact linesearch [45].

Accurate control derivatives are paramount in successfully traversing the optimization landscape, since inaccuracies (or willful approximations) yield poor search directions and may significantly slow down, altogether prevent convergence, and limit the achievable fidelity. This is particularly true for quasi-Newton methods, where successive gradients are utilized to approximate the Newton direction; gradient inaccuracies will accumulate with each iteration and completely scramble the Hessian approximation as the optimization progresses (referred to as the “slowdown” problem in Ref. [26]). Additionally, the exact Newton direction itself is typically several orders of magnitude more expensive to construct, and inaccuracies in either derivative is sure to negate any of the potential gains from the extra computational effort, discouraging its use. Finally, the

steepest descent direction is always an unattractive option, since it is well-known to have the worst general properties and convergence rate even when the exact gradient is used (linear as opposed to super-linear and quadratic for quasi-Newton and Newton directions, respectively), and any gradient inaccuracies will enhance this effect. These considerations are generic and not limited to the field of quantum control. In the following we calculate the exact derivatives for pure state transfers to surpass these issues and verify the claims and calculations by demonstration. Similar expressions are readily calculable in the density matrix formulation, which is left for future work.

A. Optimization Landscapes and Exact Derivatives

Complete specification of a control problem includes the time-evolution operator implementation as shown in the following. We will refer to the *exact* and second-order *Suzuki-Trotter* (or *Trotterized*) propagators, respectively, as

$$\hat{U}_n^{\text{Ex}} = \hat{U}_n, \quad (6)$$

$$\hat{U}_n^{\text{ST}_1} = \hat{U}_{n+1}^{c/2} \hat{U}_n^d \hat{U}_n^{c/2} = \hat{U}_n^{\text{Ex}} + \mathcal{O}(\delta t^3), \quad (7)$$

$$\hat{U}_n^{\text{ST}_2} = \hat{U}_n^{c/2} \hat{U}_n^d \hat{U}_n^{c/2} = \hat{U}_n^{\text{Ex}} + \mathcal{O}(\delta t^3), \quad (8)$$

with the definitions

$$\hat{U}_n \equiv e^{-i\hat{H}_n\delta t}, \quad \hat{U}_n^{c/2} \equiv e^{-i\hat{H}_n^c\delta t/2}, \quad \hat{U}_n^d \equiv e^{-i\hat{H}_n^d\delta t}, \quad (9)$$

in units where $\hbar = 1$. Note that the operator splitting $\hat{U}_n^{\text{ST}_1}$ entails the control points both at n and $n+1$ [50], whereas the $\hat{U}_n^{\text{ST}_2}$ splitting scheme is fully local in n with the same error [51]. Although either of these choices are valid to approximate the dynamics and appears on the same footing, their derivative calculations and final expressions are different, underscoring that the precise specification of the implementation is central for use in optimal control contexts (the approximations in derivatives should “match” those of the dynamics).

Numerically, the exact propagator corresponds to direct exponentiation of the Hamiltonian matrix, an operation that scales extremely poorly for increasing Hilbert space dimension $D_{\mathcal{H}}$. The Trotterized propagators, on the other hand, lend themselves more readily to a variety of very efficient, problem dependent implementations through e.g. the use of sparsity structures and has a much more benign Hilbert space scaling, extending its applicability far beyond the exact propagator approach. In Sec. III we will also discuss the results of this section in comparison to Krylov-Lanczos propagation, another common type of approximate time evolution.

The local $\mathcal{O}(\delta t^3)$ Trotterization errors accumulates throughout the evolution defined by Eq. (4), yielding an overall error $\mathcal{O}(\delta t^2)$. It is convenient to interpret this as

an error with respect to the (“true”) exact landscape,

$$J_F^{\text{ST}}(\vec{u}) = J_F^{\text{Ex}}(\vec{u}) + \mathcal{O}_{J_F^{\text{ST}}}(\delta t^2), \quad (10)$$

for $\text{ST} = \text{ST}_1, \text{ST}_2$. The granularity of δt determines how faithful the representation is and, in particular, it follows that geometric entities for the *same* \vec{u} are generally different in the three landscapes, e.g. the landscape height (cost value), derivatives, and thus also the search directions for optimization. Importantly, the optimal controls associated with optima in the Trotterized landscapes at large finite δt may not correspond to optima in the exact landscape, which is equivalent to the target not being obtained when propagating said controls using Eq. (6). As $\delta t \rightarrow 0$, however, the Trotterized landscapes continuously deform into the exact landscape, and below some sufficiently small finite δt they represent it with only slight modifications. As the landscapes transitively inherit the numerical implementation properties of their associated propagator, there is ample impetus for studying these proxy landscapes.

Detailed calculations of the analytically exact derivatives are given in Appendix A. The results for the gradients are

$$\frac{\partial J_F^{\text{Ex}}}{\partial u_n} = \Re \left(i o^* \langle \chi_n | \hat{H}_n^{c'} | \psi_n \rangle \right) \delta t + \mathcal{O}_{\nabla J_F^{\text{Ex}}}(\delta t^2), \quad (11)$$

$$\frac{\partial J_F^{\text{ST}_1}}{\partial u_n} = \Re \left(i o^* \langle \chi_n | \hat{H}_n^{c'} | \psi_n \rangle \right) \delta t, \quad (12)$$

$$\frac{\partial J_F^{\text{ST}_2}}{\partial u_n} = \Re \left(\frac{i o^*}{2} \sum_{p=n}^{n+1} \langle \chi_p | \hat{H}_n^{c'} | \psi_p \rangle \right) \delta t, \quad (13)$$

where $|\chi_n\rangle = \hat{U}_n^\dagger |\chi_{n+1}\rangle$ is the backwards propagated target state ($|\chi_{N_t}\rangle = |\psi_{\text{tgt}}\rangle$), $o = \langle \chi_{N_t} | \psi_{N_t} \rangle$ is the transfer amplitude, and $\hat{H}_n^{c'} = \partial \hat{H}_n^c / \partial u_n$ is the control derivative Hamiltonian. Thus, the gradients for J^{Ex} and J^{ST_1} are the same only to first order in δt : whereas $\nabla J_F^{\text{ST}_1}$ is *analytically exact* with just the δt term, ∇J_F^{Ex} entails an expensive remainder term beyond the first-order approximation. Note on the contrary that ∇J_F^{Ex} and $\nabla J_F^{\text{ST}_2}$ do *not* coincide even to first order.

Defining the recursive commutator as

$$[X, Y]_k = [X, [X, Y]_{k-1}], \quad [X, Y]_0 = Y, \quad (14)$$

the remainder term entails an infinite series,

$$\mathcal{O}_{\nabla J_F^{\text{Ex}}}(\delta t^2) \propto \left\langle \chi_n \left| \left(\sum_{k=1}^{\infty} \frac{i^k \delta t^k}{(k+1)!} [\hat{H}_n, \hat{H}_n^{c'}]_k \right) \right| \psi_n \right\rangle \delta t, \quad (15)$$

where the first-order approximation in Eq. (11) is the $k = 0$ term. In numerical application, the summation continues until machine precision or some lower desired accuracy, corresponding to some k_{max} . This is necessary because, generally, the Hamiltonian and its control derivative do not commute $[\hat{H}_n, \hat{H}_n^{c'}] \neq 0$ and the recursive commutator is not guaranteed to terminate and may

even grow (as measured by some appropriate norm) with k . A few examples include $\hat{H} = \hat{\sigma}_x + u(t) \cdot \hat{\sigma}_z$ where $\hat{\sigma}_i$ are spin operators, $\hat{H} = \hat{T} + \hat{V}(u(t))$ where \hat{V} (\hat{T}) is the potential (kinetic) energy operator for a single particle, or the Bose-Hubbard Hamiltonian $\hat{H} = -\hat{J} + \hat{U}(u(t))$ where \hat{J} (\hat{U}) is the tunneling (on-site) operator. As we shall see below, the presence of the infinite sum means that in the context of optimization, perhaps surprisingly, it may not be desirable to use exact time evolution even if it is readily available.

For the Trotterized landscapes, the calculation of $\nabla J_F^{\text{ST}_1}$ and $\nabla J_F^{\text{ST}_2}$ contains an infinite series of the same structure, but with $\hat{H}_n \rightarrow \hat{H}_n^c$ in the first argument of the recursive commutator. A central additional (mild) assumption is that the control Hamiltonian is given in its diagonal representation, in which case $[\hat{H}_n^c, \hat{H}_n^{c'}]_k = \hat{H}_n^{c'} \cdot \delta_{0,k}$ because two diagonal matrices always commute, and the series terminate after $k_{\text{max}} = 0$ exactly. Incidentally, in many cases the “natural” basis states for computations are already the ones that diagonalize \hat{H}_n^c , e.g. spin eigenstates ($|\uparrow\rangle, |\downarrow\rangle$), position eigenstates ($|\vec{x}\rangle$), or site-occupation eigenstates ($|n_i\rangle$) for the Hamiltonians mentioned above. The operator splitting and control diagonality has additional computational benefits because it disentangles and trivializes the control and drift exponential calculations: $\hat{U}_n^{c/2}$ is relatively cheap to calculate (diagonal matrix exponentiation is the element-wise exponentiation of the diagonal), and the possibly expensive calculations of \hat{U}_n^d for all n can be performed once and stored in memory or on the disk (it is by definition independent of the choice of \vec{u}). This allows significant performance boosts at runtime.

The gradient $\nabla J_F^{\text{ST}_2}$ is slightly more involved to implement than $\nabla J_F^{\text{ST}_1}$ due to the factor 2 increase in the number of overlap calculations, although this is marginal compared to the time evolution computational effort. Similar calculations and arguments apply to the analytically exact Hessians, but in this case, the expressions for $\nabla^2 J_F^{\text{Ex}}$ and $\nabla^2 J_F^{\text{ST}_2}$ are much more complicated than $\nabla^2 J_F^{\text{ST}_1}$ as shown in Appendix A.

An alternative way of calculating the exact propagator derivatives is through the auxiliary matrix method [46, 47]. Focusing on the first derivative, the relation

$$\begin{pmatrix} \hat{U}_n & \frac{\partial \hat{U}_n}{\partial u_n} \\ 0 & \hat{U}_n \end{pmatrix} = \exp \left[-i \begin{pmatrix} \hat{H}_n & \hat{H}_n^{c'} \\ 0 & \hat{H}_n \end{pmatrix} \delta t \right] \quad (16)$$

allows extraction of $\frac{\partial \hat{U}_n}{\partial u_n}$ by explicitly calculating the right hand side 2×2 block matrix exponential (the expression can be augmented to 3×3 block matrix to also include the Hessian). This approach provides exact derivatives while elegantly circumventing the cumbersome commutator series associated with the exact propagator, but the required $2D_{\mathcal{H}}$ (or $3D_{\mathcal{H}}$ with Hessian) square matrix exponentials becomes similarly expensive. Applying Trotterization and diagonal controls in combi-

nation with Eq. 16 (substitute $\hat{U}_n \rightarrow \hat{U}_n^{c/2}$ and $\hat{H}_n \rightarrow \hat{H}_n^c$) yields a very sparse, *almost* diagonal matrix for exponentiation, with a single dense-off-diagonal. Although very efficient numerical sparse solvers exist, the computation remains non-trivial, and it is always cheaper to instead utilize Eqs. (12)-(13) in this case since the exponential itself is analytically trivialized and $\hat{H}_n^{c'}$ is also on analytically closed form.

For completeness we also include derivatives for common control regularization terms (amplitude and temporal derivative) in Sec. A. These cost augmentations are often introduced for experimental reasons, and they do not depend on the numerical propagation scheme.

B. Optimizing in Exact and Control-Diagonal Trotter Landscapes

1. Two-level system

To quantitatively verify the assertions made in the previous section on concrete problems, we first consider the canonical LZ model with $\hat{H}_n = \hat{H}^d + \hat{H}_n^c = \frac{1}{2}(\hat{\sigma}_x + u_n \cdot \hat{\sigma}_z)$ and the state transfer $|\psi_{\text{ini}}\rangle = |\uparrow\rangle \rightarrow |\psi_{\text{tgt}}\rangle = |\downarrow\rangle$. This problem is already represented in the necessary control-diagonal form. The reason for choosing this minimal ($D_{\mathcal{H}} = 2$) problem in particular is twofold. First, it has well-understood solutions [52] with a single, analytical time-optimal solution $u_n = 0$ at $T_{\text{opt}} = \pi$ and remains solvable beyond this duration. Second, despite its simplicity, the model remains prototypical even in the context of many-body arena. For example, many-body dynamics can in certain scenarios be thought of as a cascade of independent LZ transitions and similar characteristics between LZ and some many-body control problems have been found [53–55].

Figure 1 shows the optimization results. From the $1-F$ iteration trajectories we find that unit fidelities (to machine precision) are easily obtainable when utilizing any of the exact gradients, with some variance in the number of iterations needed. When a solution approaches the optimum, very rapid convergence is observed. Looking, however, at the optimization wall time trajectories provides a definite performance hierarchy since two bands obtaining unit fidelity appears. The band constituted by the green and orange trajectories is separated by up to an order of magnitude in computation time from the band constituted by the purple and blue trajectories. These bands are associated with the Trotterized and exact landscapes, respectively, and the separation is due to both the difference in propagation computation time and either $k_{\text{max}} = 15$ tail in Eq. (15) or the $2D_{\mathcal{H}} \times 2D_{\mathcal{H}}$ matrix exponential in Eq. (16). As opposed to the exact gradients, the first-order gradient approximation $k_{\text{max}} = 0$ in the exact landscape performs significantly worse. It prevents convergence to unit fidelities by more than 10 orders of magnitude while also being slower compared to

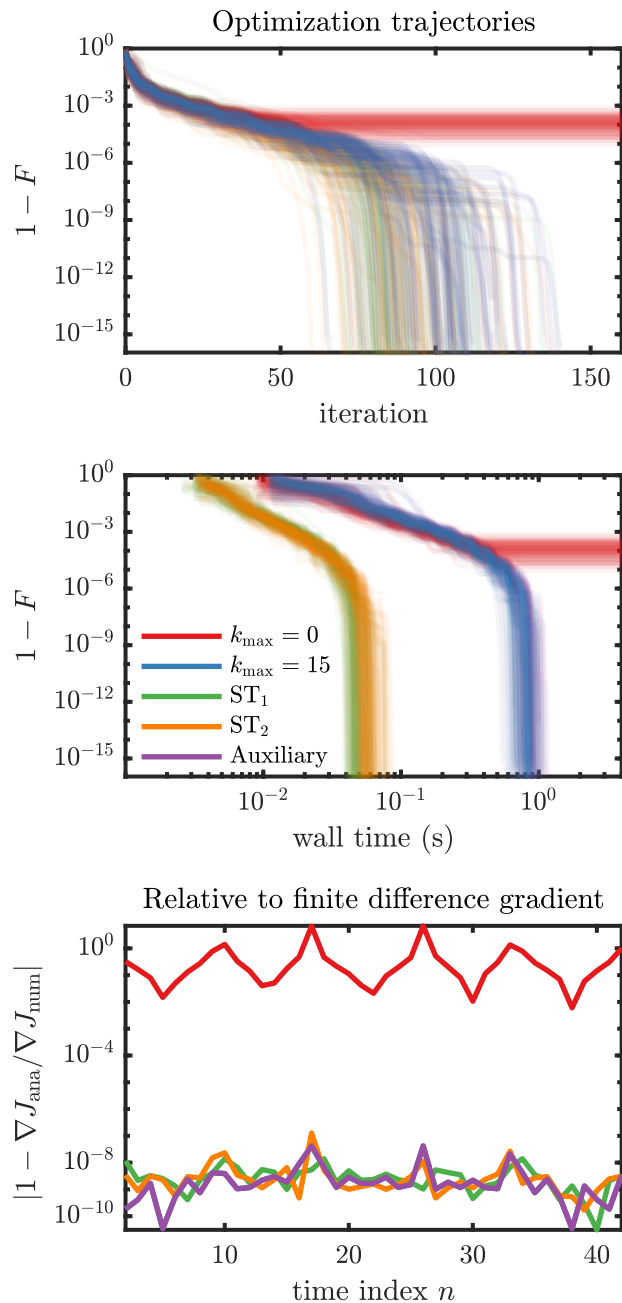


FIG. 1. Demonstration of optimizing in exact- and Trotterized landscapes for the simple two-level LZ problem. Top and middle: At $T = 1.01\pi \gtrsim T_{\text{opt}}$ with $\delta t = 0.075$ and for the same uniformly randomly generated seeds, $u_n = \text{uniform}(-20, 20)$, we optimize with the BFGS search direction (as implemented in MATLAB’s `fminunc`) in five different scenarios: exact propagator with first-order ($k_{\max} = 0$) and exact ($k_{\max} = 15$ and auxiliary method) gradients, and both Trotterized propagators with exact gradients. Out of 100 seeds, only 8 (not shown) did not converge to machine precision in 400 iterations when using exact gradients. Bottom: Analytical gradients (∇J_{ana}) relative to their numerical central finite difference approximation (∇J_{num}) with perturbation $\epsilon_{\text{pert}} = \epsilon_{\text{mach}}^{1/3}$ for a constant example control with $u_n = 5$. Note that the Auxiliary and $k_{\max} = 15$ gradients are identical to machine precision and thus yield (nearly) the same iteration trajectories, and, incidentally, wall time trajectories.

iterations in the Trotterized landscapes. Comparing the analytical gradients to numerical finite difference gradients further shows that the first-order approximation can be very poor, whereas the exact ones are in close agreement. Note that the central finite difference gradients themselves are associated with errors of order $\mathcal{O}_{\nabla J_F}(\delta t^2)$, and the relative differences are on the order $\sqrt{\epsilon_{\text{mach}}}$ where $\epsilon_{\text{mach}} = 2.22 \cdot 10^{-16}$ is the machine precision for the double-precision floating-point format.

For simplicity, we chose a static truncation parameter in this example such that $\delta t^{k_{\max}} \lesssim \epsilon_{\text{mach}}$. With decreasing δt , the necessary k_{\max} for exact gradients also decreases and the $k = 0$ term becomes increasingly dominant. Indeed, running the same optimizations as in Fig. 1 for $\delta t = 0.025$, the $k_{\max} = 0$ optimization yields 2-3 orders of magnitude better final results, and at $\delta t = 0.01$ the first-order approximation is sufficient for finding machine precision unit fidelities. That is, reducing the number of k terms required for accurate gradients is traded off for increased computation time per iteration due to additional time evolutions. As a consequence of the much larger computational overheads in computing the exact matrix exponential, the $k_{\max} = 0$ trajectories remains similarly separated from the Trotterized trajectories even though it may now be sufficient in terms of final results. We also tried $k_{\max} = 9$, the smallest such that $\delta t^{k_{\max}} / (k_{\max} + 1)! \lesssim \epsilon_{\text{mach}}$ and a dynamic scheme (since the recursive commutator depends on u_n) based on the infinity norm of subsequent terms being smaller than ϵ_{mach} and found virtually no difference to the presented results. It is expected that the dynamic scheme in particular may be more appropriate outside of this minimal problem, and we employ this in the next example. It is also likely that a less conservative summation cut-off threshold $\epsilon < \epsilon_{\text{mach}}$ may be used. In any event, the question of the best strategy for choosing the smallest k_{\max} that produces sufficiently exact gradients depends intimately on the problem (or rather, its representation) at hand and its parameters, and there may not be a definite answer. This also illuminates that analytical scaling comparisons to the auxiliary matrix method Eq.(16) are not immediately obvious in general. Incidentally, we find that the auxiliary and $k_{\max} = 15$ exact gradients have virtually the same wall time performances in this problem.

2. Transmon system

We now turn to a second example of higher dimensionality ($D_{\mathcal{H}} = 9$), a superconducting transmon system with two-qutrit Hamiltonian

$$\hat{H}_n = \left[\Delta \hat{b}_1^\dagger \hat{b}_1 + \frac{1}{2} \sum_{j=1,2} \delta_j \hat{b}_j^\dagger \hat{b}_j (\hat{b}_j^\dagger \hat{b}_j - 1) + J(\hat{b}_1^\dagger \hat{b}_2 + \hat{b}_1 \hat{b}_2^\dagger) \right] + u_n(\hat{b}_1^\dagger + \hat{b}_1) = \hat{H}^d + \hat{H}_n^c, \quad (17)$$

with the same parameter values as in Ref. [56]. We consider the state transfer $|\psi_{\text{ini}}\rangle = |10\rangle \rightarrow |\psi_{\text{tgt}}\rangle = |11\rangle$, i.e. a single state mapping of a CNOT gate in the computational qubit subspace $\{|00\rangle, |01\rangle, |10\rangle, |11\rangle\}$, without control constraints. This process is expected to have a lower quantum speed limit than what we found for the full gate [56]. (The full CNOT could have been considered in the state transfer formulation by optimizing a composite cost, e.g. $J_F^{[00]\rightarrow[00]} + J_F^{[01]\rightarrow[01]} + J_F^{[11]\rightarrow[10]} + J_F^{[10]\rightarrow[11]}$.) Note that the control Hamiltonian is not diagonal in the (natural) computational basis. To obtain a proper representation for the Trotter exact derivatives we therefore numerically diagonalize $\hat{H}_n^c = u_n(\hat{b}_1^\dagger + \hat{b}_1)$ for some value of $u_n \neq 0$, store the eigenvectors as columns in the basis transformation operator $\hat{\mathcal{R}}$, and perform the basis change,

$$\hat{H}_n^c \leftarrow \hat{\mathcal{R}}^\dagger \hat{H}_n^c \hat{\mathcal{R}}, \quad \hat{H}^d \leftarrow \hat{\mathcal{R}}^\dagger \hat{H}^d \hat{\mathcal{R}}, \quad (18)$$

$$|\psi_{\text{ini}}\rangle \leftarrow \hat{\mathcal{R}}^\dagger |\psi_{\text{ini}}\rangle, \quad |\psi_{\text{tgt}}\rangle \leftarrow \hat{\mathcal{R}}^\dagger |\psi_{\text{tgt}}\rangle. \quad (19)$$

The results of optimizing this control-diagonalized problem is shown in Fig. 2. We find a nearly identical situation to Fig. 1, except the gap between control diagonalized Trotter and exact propagator gradient methods has significantly increased (note log-scale) due to the increased $D_{\mathcal{H}}$. Further, the first order approximation (falsely) converges more rapidly to even worse fidelities. In this example, we used an adaptive scheme for choosing k_{max} based on the infinity norm of the residual, which may explain the slightly faster optimization traces compared to the auxiliary method. Otherwise, the conclusions from the two-level example are reinforced.

III. DISCUSSION AND OUTLOOK

We discussed how and why accurate derivatives are central to achieve high fidelities and convergence rates in derivative-based methods for generic optimization tasks. We examined three common choices of time evolution scheme, the exact- and two second-order Suzuki-Trotter expanded propagators, showed how these can be interpreted and related in terms of optimization landscapes, and found by novel calculations their resulting analytically exact derivatives to differ vastly in complexity. By assuming a diagonal control Hamiltonian for the Trotterized landscape, we circumvented a detrimental infinite series, and highlighted many additional attractive properties compared to the exact landscape, among others the extended range of applicability with respect to system size. In a certain sense, when balancing respective errors in the dynamics and in the derivative calculations, the latter is more important. We demonstrated the main ideas by considering two problems of varying Hilbert space size and in both instances found the expected performance hierarchies: the control-diagonal Trotter exact derivatives lead to order(s) of magnitude

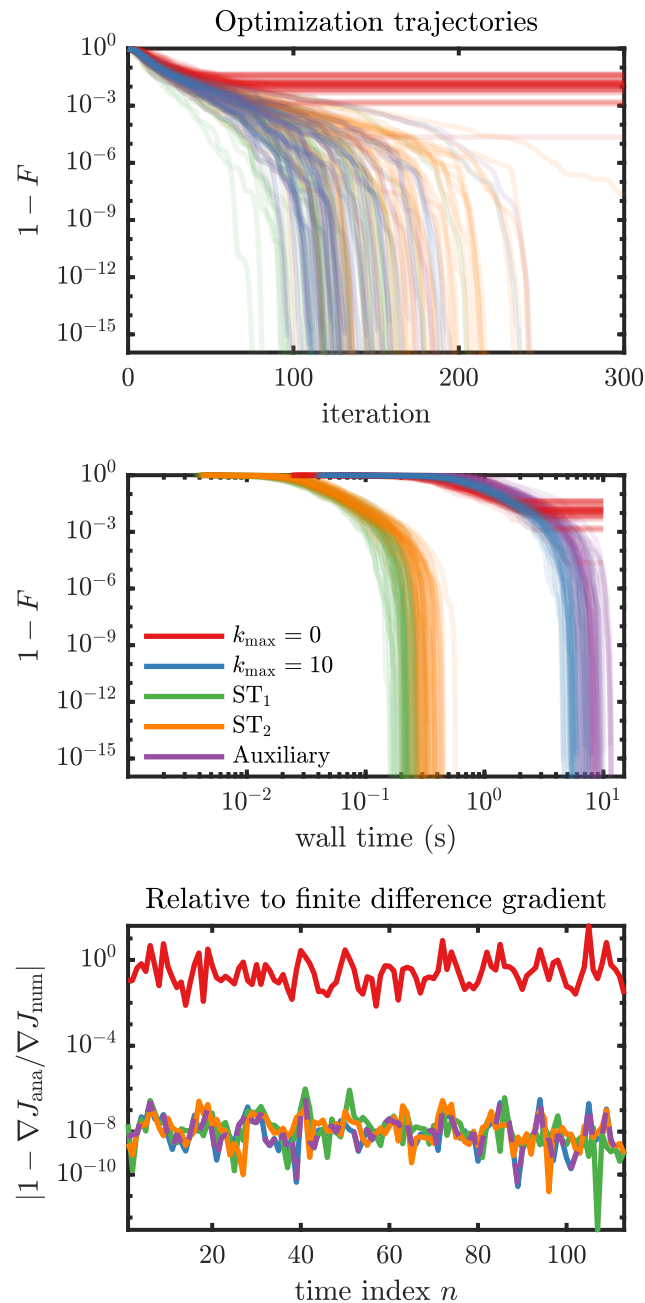


FIG. 2. Same as Fig. 1 for 50 seeds, but for the transmon system Eqs. (17)-(19) with $T = 2.83$ (50 ns) and $\delta t = 0.025$ (0.442 ns) given in non-dimensionalized numerical units and SI-units, respectively (energy is measured in units of $|J| \approx -5.97 \cdot 10^{-27}$ J and time in $\hbar/|J| \approx 17.7$ ns).

increase in computational speed and high-fidelity results (unit to machine precision).

The immediate advantages of optimizing in the Trotterized landscapes over the exact landscape are twofold: (i) they are applicable to much larger systems, and (ii) their analytically exact control derivatives and thus search directions (essential for optimization convergence)

are greatly simplified under an assumption that can always be (and often is automatically) fulfilled. The only implicit requirement is that δt is small enough for the Trotterization to faithfully approximate the exact dynamics, or equivalently the exact landscape Eq. (10). Note, however, that the exact Trotter derivatives are irrespective of δt in terms of complexity. This allows among others effective use of *homotopy* methods [50] in δt , that is, optimization on an increasingly finer time resolution. This can be used to significantly speed up initial iterations without loss of final dynamics accuracy (the error is on order $\mathcal{O}(\delta t^2)$), because the (quasi-)continuous deformation of δt can be made arbitrarily small at the end. The exact propagator can, nonetheless, still be used if the Hilbert space is sufficiently low-dimensional such that the direct exponentiation and series summation or auxiliary matrix exponentiation is feasible. However, even for the simplest possible non-trivial problem in Fig. 1 this approach is seen to be much slower than the alternative. This difference in computational feasibility increases monotonically with the Hilbert space dimensionality as evidenced by Fig. 2. These main conclusions are summarized in Table I. The aggregate computational performance of our control-diagonal Trotter methodology, including the homotopy, provides a scaffolding for efficient derivative-based optimization of very high-dimensional many-body dynamics in the high-fidelity limit. We pursue this in parallel work [57] for a system far beyond exact diagonalization approaches, necessitating a matrix product state description.

Another common way of approximating the time-evolution for extended applicability is through the use of Krylov-Lanczos subspace methods [58–60] where operator applications like $\hat{U}_n |\psi_n\rangle$ or $\frac{\partial \hat{U}_n}{\partial u_n} |\psi_n\rangle$ are calculated without explicit construction of the operator exponentials. Here we briefly compare this approach with our Trotterized control diagonal scheme. For example, numerically stepping forward in time $|\psi_{n+1}\rangle = \hat{U}_n |\psi_n\rangle$ with Krylov-Lanczos entails (i) iterative construction of $k \leq D_{\mathcal{H}}$ Lanczos vectors q_i of dimension $D_{\mathcal{H}}$ each requiring a matrix-vector multiplication on the form $\hat{H}_n q_i$ as the most expensive operation, and (ii) matrix exponentiation of a $k \times k$ matrix and at least another matrix multiplication. This turns out to be computationally efficient compared to exact propagation when $k \ll D_{\mathcal{H}} \gg 1$, where k controls the approximation accuracy. The control diagonal Trotter steps e.g. $|\psi_{n+1}\rangle = \hat{U}_n^{c/2} \hat{U}_n^d \hat{U}_n^{c/2} |\psi_n\rangle$ numerically requires (naïvely) a total of 3 matrix multiplications. However, because $\hat{U}_n^{c/2}$ is diagonal, the exponentiation of each diagonal element can be efficiently stored in a vector and a total of two elementwise vector-vector multiplications needs to be performed for the control part. For the drift part, recall \hat{U}_n^d only needs to be calculated once and can be cached indefinitely, leaving only a matrix-vector multiplication with the same cost as constructing a *single* Lanczos vector. Thus, alone constructing the Lanczos vectors (i) for $k > 1$ is more costly than perform-

	Applicability	Landscape error	Derivative error
\hat{U}^{Ex}	Small systems	Exact	$\mathcal{O}(\delta t^2)^*$
\hat{U}^{ST}	“Any”	$\mathcal{O}(\delta t^2)$	Exact

TABLE I. The exact- and Trotterized propagator properties where ST = ST₁, ST₂ and the ‘*’ assumes the first-order approximation (truncation to $k_{\text{max}} = 0$ in Eq. (11)). The exact propagator is feasible only for small systems due to the direct operator exponentiation. The derivatives in the Trotterized landscapes are exactly calculable under diagonal assumptions while simultaneously having a greatly reduced computational cost regardless of system size and value of δt . Exact derivatives are very important for convergence as evidenced by the examples Figs. 1-2

ing the full Trotter step. Further, the Krylov-Lanczos procedure obfuscates the direct analytical dependence on the control u_n , disallowing a straightforward analytical derivative calculation and one must therefore use e.g. the auxiliary matrix method which implicitly assumes exact propagation. As opposed to the control diagonal Trotterization, this leads to a “mismatch” between the optimization landscape (Krylov dynamics) and the derivative calculations (exact dynamics) unless k is large enough to ensure coincidence close to machine precision. Additionally, since Krylov-Lanczos methods calculates the exponential operator *application* $e^{\hat{A}} |\psi\rangle$ rather than $e^{\hat{A}}$ itself, these cannot be used to evaluate the auxiliary matrix exponential in Eq. 16. Nevertheless, Krylov propagation is much preferable to exact propagation even for moderate values of $D_{\mathcal{H}}$.

The exact Hessian has strong theoretical properties as discussed in Sec. II, and although our new calculations of the exact Hessian have been verified numerically, we found did not yet perform comparative studies and leave this to future work. Nevertheless, we have found in a parallel, similar work that a novel calculation of the exact Hessian in the unitary gate synthesis setting [56] outperforms a gradient-only quasi-Newton approach in terms of statistics and best results in certain domains. This highly suggests similar possibilities in the present case.

Lastly, we would like to point out that the results in this paper followed a discretize-then-optimize (discretization before ordinary vector derivatives of a cost function) rather than optimize-then-discretize (discretization after continuous Gâteaux derivatives of a cost functional) approach. Since these approaches do not in general necessarily yield the same derivative expressions, the former approach is preferable because it specifically takes into account the chosen propagation scheme implementation (the derivatives “match” the landscape/dynamics) which has been a main point throughout. (Similarly, applying of Krylov subspace methods for the time-evolution while using exact gradients for the exact propagator constitutes another potential mismatch between the derivatives and landscape/dynamics.) It is therefore quite a happy coincidence that e.g. (i) the exact propagator

gradient ∇J_F^{Ex} calculated by the optimize-then-discretize approach yields exactly the same expression as $\nabla J_F^{\text{ST}_1}$, and (ii) $\hat{\mathcal{U}}^{\text{ST}_1}$ is a standard propagator for many systems, e.g. for wave functions in real space. The combined effect is that the sought after exactness of the derivatives are obtained by virtue of standard methods alone in these situations, knowingly or otherwise. Note that the same would not be true if $\hat{\mathcal{U}}^{\text{Ex}}$ or $\hat{\mathcal{U}}^{\text{ST}_2}$ was used.

IV. ACKNOWLEDGEMENTS

We thank I. Kuprov for useful discussions. This work was funded by the ERC, H2020 grant 639560 (MEC-TRL), and the John Templeton and Carlsberg Foundations.

Appendix A: Derivation of Exact Gradients and Hessians

Here we present the calculations leading to the exact gradient and Hessian expressions for both the exact propagator and the Trotterized propagators with a diagonal control Hamiltonian defined in Eqs. (6)-(8). We also define the regularization cost functionals and calculate likewise calculate their derivatives after discretization. Emphasis is put on thoroughness of the steps, and relevant equations for the derivations are re-stated for convenience where applicable, so as to be self-contained.

We assume a piecewise constant control $u(t)$ on a regularly spaced time grid $t \in [t_1, t_2, \dots, t_{N_t}] = [0, \delta t, \dots, T]$. Recall $|\psi_1\rangle = |\psi_{\text{ini}}\rangle$ and $|\psi_{N_t}\rangle = |\psi(T)\rangle$, and $\hat{H}(u_n) = \hat{H}_n = \hat{H}_n^d + \hat{H}_n^c$ where \hat{H}_n^c (\hat{H}_n^d) is the control (drift) Hamiltonian. Define the auxilliary state $|\chi_{N_t}\rangle = |\psi_{\text{tgt}}\rangle$, the transfer amplitude $o = \langle \psi_{\text{tgt}} | \psi(T) \rangle = \langle \chi_{N_t} | \psi_{N_t} \rangle$.

1. Derivatives for Exact Propagator

The exact propagator has the form $\hat{\mathcal{U}}_n = \exp(-i\hat{H}(u_n)\delta t)$ where the ^{Ex} superscript is omitted for brevity in most of the steps. It is convenient to write

$$F = |\langle \psi_{\text{tgt}} | \psi(T) \rangle|^2 = o^* o, \quad (\text{A1})$$

$$\frac{\partial J_F^{\text{Ex}}}{\partial u_n} = -\Re \left(o^* \frac{\partial o}{\partial u_n} \right), \quad (\text{A2})$$

with the overlap o and its derivative being

$$o = \langle \psi_{\text{tgt}} | \psi(T) \rangle = \left\langle \chi_{N_t} \left| \hat{\mathcal{U}}_{N_t-1} \dots \hat{\mathcal{U}}_n \dots \hat{\mathcal{U}}_1 \right| \psi_1 \right\rangle, \quad (\text{A3})$$

$$\frac{\partial o}{\partial u_n} = \left\langle \chi_{N_t} \left| \hat{\mathcal{U}}_{N_t-1} \dots \frac{\partial \hat{\mathcal{U}}_n}{\partial u_n} \dots \hat{\mathcal{U}}_1 \right| \psi_1 \right\rangle \quad (\text{A4})$$

$$= \left\langle \chi_{n+1} \left| \frac{\partial \hat{\mathcal{U}}_n}{\partial u_n} \right| \psi_n \right\rangle. \quad (\text{A5})$$

The task is then to calculate $\frac{\partial \hat{\mathcal{U}}_n}{\partial u_n}$ and be careful with ordering. Define the control derivative $H'_n \equiv \frac{\partial \hat{H}_n}{\partial u_n}$ and expand the exponential

$$\begin{aligned} \frac{\partial \hat{\mathcal{U}}_n}{\partial u_n} &= \frac{\partial}{\partial u_n} \left(e^{-i\hat{H}_n \delta t} \right) = \sum_{p=0}^{\infty} \frac{(-i\delta t)^p}{p!} \frac{\partial}{\partial u_n} \left(\hat{H}_n^p \right) \\ &= \sum_{p=1}^{\infty} \frac{(-i\delta t)^p}{p!} \sum_{q=0}^{p-1} \hat{H}_n^q \hat{H}'_n \hat{H}_n^{p-q-1}, \end{aligned} \quad (\text{A6})$$

Define for momentary simplicity $A \equiv -i\hat{H}_n \delta t$ and $B \equiv -i\hat{H}'_n \delta t$. Then it can be shown that

$$\frac{\partial \hat{\mathcal{U}}_n}{\partial u_n} = \sum_{p=0}^{\infty} \sum_{q=0}^{\infty} \frac{A^p B A^q}{(p+q+1)!}. \quad (\text{A7})$$

Using now the following relations for the Beta and Gamma functions [61]:

$$\Gamma(a) = (n-1)! \quad (\text{for } a \in \mathbb{Z}^+), \quad (\text{A8})$$

$$\begin{aligned} \beta(a, b) &= \int_0^1 (1-\alpha)^{a-1} \alpha^{b-1} d\alpha = \frac{\Gamma(a)\Gamma(b)}{\Gamma(a+b)} \\ &= \frac{(a-1)!(b-1)!}{(a+b-1)!} = \frac{p!q!}{(p+q+1)!}, \end{aligned} \quad (\text{A9})$$

and taking $a = p+1$, $b = q+1$ we obtain

$$\frac{1}{(p+q+1)!} = \frac{1}{p!q!} \int_0^1 (1-\alpha)^p \alpha^q d\alpha. \quad (\text{A10})$$

Inserting this, and initially pulling out the integral we obtain

$$\begin{aligned} \frac{\partial \hat{\mathcal{U}}_n}{\partial u_n} &= \sum_{p=0}^{\infty} \sum_{q=0}^{\infty} \frac{A^p B A^q}{p!q!} \int_0^1 \alpha^p (1-\alpha)^q d\alpha \\ &= \int_0^1 \left(\sum_{p=0}^{\infty} \frac{((1-\alpha)A)^p}{p!} \right) B \sum_{q=0}^{\infty} \frac{(\alpha A)^q}{q!} d\alpha \\ &= \int_0^1 e^{(1-\alpha)A} B e^{\alpha A} d\alpha = e^A \int_0^1 e^{-\alpha A} B e^{\alpha A} d\alpha \\ &= \hat{\mathcal{U}}_n \int_0^1 e^{(i\alpha\delta t)\hat{H}_n} (-i\delta t \hat{H}'_n) e^{-(i\alpha\delta t)\hat{H}_n} d\alpha. \end{aligned} \quad (\text{A11})$$

The integrand can be evaluated by defining the recursive commutator with base case $[c_x X, c_y Y]_0 = c_y Y$ as in the

main text and using Baker-Campbell-Hausdorff relations [62]

$$[c_x X, c_y Y]_k = [c_x X, [c_x X, c_y Y]_{k-1}] = c_x^k c_y [X, Y]_k, \quad (\text{A12})$$

$$e^{c_x X} Y e^{-c_x X} = \sum_{k=0}^{\infty} \frac{[c_x X, c_y Y]_k}{k!} = \sum_{k=0}^{\infty} \frac{c_x^k c_y}{k!} [X, Y]_k, \quad (\text{A13})$$

by evaluating these with scalars $c_x = i\alpha\delta t$ and $c_y = -i\delta t$

$$\begin{aligned} \frac{\partial \hat{\mathcal{U}}_n}{\partial u_n} &= \hat{\mathcal{U}}_n \int_0^1 \left(\sum_{k=0}^{\infty} \frac{(i\alpha\delta t)^k (-i\delta t)}{k!} [\hat{H}_n, \hat{H}'_n]_k d\alpha \right) \\ &= \hat{\mathcal{U}}_n \sum_{k=0}^{\infty} (-i\delta t) \frac{i^k \delta t^k}{k!} [\hat{H}_n, \hat{H}'_n]_k \left(\int_0^1 \alpha^k d\alpha \right) \\ &= \hat{\mathcal{U}}_n (-i\delta t) \sum_{k=0}^{\infty} \frac{i^k \delta t^k}{(k+1)!} [\hat{H}_n, \hat{H}'_n]_k. \end{aligned} \quad (\text{A14})$$

Substituting this into Eq. (A5), the resulting expression into Eq. (A2), and using $\hat{H}_n = \hat{H}_n^{c'}$ gives

$$\begin{aligned} \frac{\partial J_F^{\text{Ex}}}{\partial u_n} &= \Re \left(i o^* \left\langle \chi_n \left| \left(\sum_{k=0}^{\infty} \frac{i^k \delta t^k}{(k+1)!} [\hat{H}_n, \hat{H}_n^{c'}]_k \right) \right| \psi_n \right\rangle \right) \delta t \\ &= \Re \left(i o^* \left\langle \chi_n \left| \hat{H}_n^{c'} \right| \psi_n \right\rangle \right) \delta t + \mathcal{O}_{\nabla J_F}(\delta t^2). \end{aligned} \quad (\text{A16})$$

which is the expression stated in (11).

To calculate the Hessian, we take the derivative of Eq. (A2)

$$\frac{\partial^2 J_F^{\text{Ex}}}{\partial u_n \partial u_m} = -\Re \left(\left(\frac{\partial o}{\partial u_m} \right)^* \frac{\partial o}{\partial u_n} + o^* \frac{\partial^2 o}{\partial u_n \partial u_m} \right). \quad (\text{A17})$$

This form is valid for both the exact and Trotterized propagator. We recall previous definitions with an additional index m highlighted:

$$o = \langle \chi_{N_t} | \hat{\mathcal{U}}_{N_t-1} \dots \hat{\mathcal{U}}_n \dots \hat{\mathcal{U}}_m \dots, \hat{\mathcal{U}}_1 | \psi_1 \rangle, \quad (\text{A18})$$

$$\begin{aligned} \frac{\partial o}{\partial u_n} &= \langle \chi_{N_t} | \hat{\mathcal{U}}_{N_t-1} \dots \frac{\partial \hat{\mathcal{U}}_n}{\partial u_n} \dots \hat{\mathcal{U}}_m \dots, \hat{\mathcal{U}}_1 | \psi_1 \rangle \\ &= \langle \chi_{n+1} | \frac{\partial \hat{\mathcal{U}}_n}{\partial u_n} | \psi_n \rangle. \end{aligned} \quad (\text{A19})$$

With the gradient at hand, the Hessian calculation thus only needs additional evaluation of the second derivatives

of o ,

$n > m$:

$$\begin{aligned} \frac{\partial^2 o}{\partial u_n \partial u_m} &= \langle \chi_{N_t} | \hat{\mathcal{U}}_{N_t-1} \dots \frac{\partial \hat{\mathcal{U}}_n}{\partial u_n} \dots \frac{\partial \hat{\mathcal{U}}_m}{\partial u_m} \dots \hat{\mathcal{U}}_1 | \psi_1 \rangle \\ &= \langle \chi_{n+1} | \frac{\partial \hat{\mathcal{U}}_n}{\partial u_n} \left(\prod_{j=m+1}^{n-1} \hat{\mathcal{U}}_j \right) \frac{\partial \hat{\mathcal{U}}_m}{\partial u_m} | \psi_m \rangle, \end{aligned} \quad (\text{A20a})$$

$n = m$:

$$\begin{aligned} \frac{\partial^2 o}{\partial u_n \partial u_m} &= \langle \chi_{N_t} | \hat{\mathcal{U}}_{N_t-1} \dots \frac{\partial^2 \hat{\mathcal{U}}_n}{\partial u_n^2} \dots \hat{\mathcal{U}}_1 | \psi_1 \rangle \\ &= \langle \chi_{n+1} | \frac{\partial^2 \hat{\mathcal{U}}_n}{\partial u_n^2} | \psi_n \rangle. \end{aligned} \quad (\text{A20b})$$

The case $m > n$ is the same as $n > m$ with indices $n \leftrightarrow m$ (we need only calculate one of the cases due to symmetry). Inserting these expressions in Eq. (A17) we obtain the exact Hessian elements $n \geq m$ (without loss of generality) for the exact propagator

$$\begin{aligned} \frac{\partial^2 J_F^{\text{Ex}}}{\partial u_n \partial u_m} &= -\Re \left(\langle \psi_m | \frac{\partial \hat{\mathcal{U}}_m}{\partial u_m} | \chi_{m+1} \rangle \langle \chi_{n+1} | \frac{\partial \hat{\mathcal{U}}_n}{\partial u_n} | \psi_n \rangle \right) \\ &\quad - \Re \left(o^* \langle \chi_{n+1} | \frac{\partial \hat{\mathcal{U}}_n}{\partial u_n} \left(\prod_{j=m+1}^{n-1} \hat{\mathcal{U}}_j \right) \frac{\partial \hat{\mathcal{U}}_m}{\partial u_m} | \psi_m \rangle \right) (1 - \delta_{n,m}) \\ &\quad - \Re \left(o^* \langle \chi_{n+1} | \frac{\partial^2 \hat{\mathcal{U}}_n}{\partial u_n^2} | \psi_n \rangle \right) \delta_{n,m} \end{aligned} \quad (\text{A21})$$

where $\frac{\partial \hat{\mathcal{U}}_n}{\partial u_n}$ is given by Eq. (A14). Evaluating $\frac{\partial^2 \hat{\mathcal{U}}_n}{\partial u_n^2}$ is straightforward,

$$\begin{aligned} \frac{\partial^2 \hat{\mathcal{U}}_n}{\partial u_n^2} &= \hat{\mathcal{U}}_n \left\{ \left(-i\delta t \sum_{k=0}^{\infty} \frac{i^k \delta t^k}{(k+1)!} [\hat{H}_n, \hat{H}'_n]_k \right)^2 \right. \\ &\quad \left. - i\delta t \sum_{k=0}^{\infty} \frac{i^k \delta t^k}{(k+1)!} [\hat{H}_n, \hat{H}'_n]_k \right\}, \end{aligned} \quad (\text{A22})$$

but the recursive commutator derivative is cumbersome

$$[\hat{H}_n, \hat{H}'_n]_k' = [\hat{H}_n, [\hat{H}_n, \hat{H}'_n]_{k-1}'] - [\hat{H}'_n, [\hat{H}_n, \hat{H}'_n]_{k-1}] \quad (\text{A23a})$$

$$\begin{aligned} [\hat{H}_n, \hat{H}'_n]_0' &= \hat{H}_n'', \\ [\hat{H}_n, \hat{H}'_n]_1' &= [\hat{H}_n, \hat{H}_n''], \\ [\hat{H}_n, \hat{H}'_n]_2' &= [\hat{H}_n, [\hat{H}_n, \hat{H}_n'']] + [\hat{H}_n', [\hat{H}_n, \hat{H}_n']], \\ &\vdots \end{aligned}$$

where we explicitly evaluated the first few terms. Note that the exact derivatives both entail an infinite summation (machine precision in finite arithmetic).

2. Derivatives for Trotterized Propagators

We consider now in turn the Suzuki-Trotter expansions $\hat{U}_n^{\text{ST}_1} = \hat{U}_{n+1}^{c/2} \hat{U}_n^d \hat{U}_n^{c/2}$ and $\hat{U}_n^{\text{ST}_2} = \hat{U}_n^{c/2} \hat{U}_n^d \hat{U}_n^{c/2}$ where $\hat{U}_n^{c/2} \equiv e^{-i\hat{H}_n^c \delta t/2}$ and $\hat{U}_n^d \equiv e^{-i\hat{H}_n^d \delta t}$.

a. Derivatives of $\hat{U}_n^{\text{ST}_1}$

For the Suzuki-Trotter expansion $\hat{U}_n^{\text{ST}} = \hat{U}_{n+1}^{c/2} \hat{U}_n^d \hat{U}_n^{c/2}$ the control dependence is distributed among n and $n-1$ (except at the end points $n = 1, N$), yielding

$$\frac{\partial J_F^{\text{ST}_1}}{\partial u_n} = -\Re \left(o^* \frac{\partial o}{\partial u_n} \right), \quad (\text{A24a})$$

$$\frac{\partial o}{\partial u_n} = \left\langle \chi_{n+1} \left| \frac{\partial}{\partial u_n} \left(\hat{U}_n^{\text{ST}_1} \hat{U}_{n-1}^{\text{ST}_1} \right) \right| \psi_{n-1} \right\rangle. \quad (\text{A24b})$$

Additionally, assume that the control Hamiltonian is diagonal. We use Eq. (A14) to take the derivative of $(\hat{U}_n^{\text{ST}_1} \hat{U}_{n-1}^{\text{ST}_1})$,

$$\begin{aligned} \frac{\partial}{\partial u_n} (\hat{U}_n^{\text{ST}_1} \hat{U}_{n-1}^{\text{ST}_1}) &= \frac{\partial}{\partial u_n} \left((\hat{U}_{n+1}^{c/2} \hat{U}_n^d \hat{U}_n^{c/2}) (\hat{U}_n^{c/2} \hat{U}_{n-1}^d \hat{U}_{n-1}^{c/2}) \right) \\ &= (\hat{U}_{n+1}^{c/2} \hat{U}_n^d) \frac{\partial \hat{U}_n^c}{\partial u_n} (\hat{U}_{n-1}^d \hat{U}_{n-1}^{c/2}) \\ &= (\hat{U}_{n+1}^{c/2} \hat{U}_n^d) \left\{ \hat{U}_n^c (-i\delta t \hat{H}_n^{c'}) \right\} (\hat{U}_{n-1}^d \hat{U}_{n-1}^{c/2}) \\ &= (-i\delta t) \cdot (\hat{U}_{n+1}^{c/2} \hat{U}_n^d \hat{U}_n^{c/2}) \hat{H}_n^{c'} (\hat{U}_n^{c/2} \hat{U}_{n-1}^d \hat{U}_{n-1}^{c/2}) \\ &= (-i\delta t) \cdot \hat{U}_n^{\text{ST}_1} \hat{H}_n^{c'} \hat{U}_{n-1}^{\text{ST}_1}. \end{aligned} \quad (\text{A25})$$

Here we also used that two diagonal matrices always commute, first to evaluate the recursive commutator $[\hat{H}_n^c, \hat{H}_n^{c'}]_k = \hat{H}_n^{c'} \cdot \delta_{0,k}$ from (A14), and second to recombine the initial propagators since $[H_n^{c'}, \hat{U}_n^{c/2}] = 0$. Inserting into (A24a)-(A24b) yields the exact gradient stated in Eq. (12),

$$\frac{\partial J_F^{\text{ST}}}{\partial u_n} = \Re \left(i o^* \left\langle \chi_n \left| H_n^{c'} \right| \psi_n \right\rangle \right) \delta t, \quad (\text{A26})$$

with an additional factor 1/2 at the end points ($n = 1, N_t$). Apart from these, this is identical to exact propagator gradient Eq. (11) when in the first-order approximation $k_{\text{max}} = 0$, i.e. discarding the otherwise expensive $\mathcal{O}(\delta t^2)$ tail.

The Hessian elements are written as

$$\frac{\partial^2 J_F}{\partial u_n \partial u_m} = -\Re \left(\left(\frac{\partial o}{\partial u_m} \right)^* \frac{\partial o}{\partial u_n} + o^* \frac{\partial^2 o}{\partial u_n \partial u_m} \right). \quad (\text{A27})$$

The second derivatives to be calculated are

$n > m :$

$$\frac{\partial^2 o}{\partial u_n \partial u_m} = \langle \chi_{n+1} | \frac{\partial}{\partial u_n} \left(\hat{U}_n^{\text{ST}} \hat{U}_{n-1}^{\text{ST}} \right) \left(\prod_{j=m+1}^{n-2} \hat{U}_j \right) \frac{\partial}{\partial u_m} \left(\hat{U}_m^{\text{ST}} \hat{U}_{m-1}^{\text{ST}} \right) | \psi_{m-1} \rangle, \quad (\text{A28a})$$

$n = m :$

$$\frac{\partial^2 o}{\partial u_n \partial u_m} = \langle \chi_{n+1} | \frac{\partial^2}{\partial u_n^2} \left(\hat{U}_n^{\text{ST}} \hat{U}_{n-1}^{\text{ST}} \right) | \psi_{n-1} \rangle. \quad (\text{A28b})$$

For $n > m$ we only need the first derivative given in Eq. (A25). For $n = m$ we take the second derivative of $(\hat{U}_n^{\text{ST}} \hat{U}_{n-1}^{\text{ST}})$ using Eq. (A25) and commutation relations due to diagonal H_n^c

$$\begin{aligned} \frac{\partial^2}{\partial u_n^2} (\hat{U}_n^{\text{ST}} \hat{U}_{n-1}^{\text{ST}}) &= (-i\delta t) \frac{\partial}{\partial u_n} \left(\hat{U}_n^{\text{ST}} \hat{H}_n^{c'} \hat{U}_{n-1}^{\text{ST}} \right) \\ &= (-i\delta t) \hat{U}_{n+1}^{c/2} \hat{U}_n^d \frac{\partial}{\partial u_n} \left(\hat{U}_n^c \hat{H}_n^{c'} \right) \hat{U}_{n-1}^d \hat{U}_{n-1}^{c/2} \\ &= (-i\delta t) \hat{U}_{n+1}^{c/2} \hat{U}_n^d \left(\hat{U}_n^c (-i\delta t \hat{H}_n^{c'}) \hat{H}_n^{c'} + \hat{U}_n^c \hat{H}_n^{c''} \right) \hat{U}_{n-1}^d \hat{U}_{n-1}^{c/2} \\ &= (-i\delta t) \hat{U}_{n+1}^{c/2} \hat{U}_n^d \hat{U}_n^{c/2} \left(\hat{H}_n^{c''} - i\delta t (\hat{H}_n^{c'})^2 \right) \hat{U}_n^{c/2} \hat{U}_{n-1}^d \hat{U}_{n-1}^{c/2} \\ &= (-i\delta t) \cdot \hat{U}_n^{\text{ST}} \left(\hat{H}_n^{c''} - i\delta t (\hat{H}_n^{c'})^2 \right) \hat{U}_{n-1}^{\text{ST}}. \end{aligned} \quad (\text{A29})$$

The exact Hessian elements $n \geq m$ for this Trotterization scheme are therefore

$$\begin{aligned} \frac{\partial^2 J_F^{\text{ST}_1}}{\partial u_n \partial u_m} &= -\Re \left(\left\langle \psi_m \left| \hat{H}_m^{c'} \right| \chi_m \right\rangle \cdot \left\langle \chi_n \left| \hat{H}_n^{c'} \right| \psi_n \right\rangle \right) \delta t^2 \\ &+ \Re \left(o^* \langle \chi_n | \hat{H}_n^{c'} \left(\prod_{j=m+1}^n \hat{U}_j \right) \hat{H}_m^{c'} | \psi_m \rangle \right) \delta t^2 \cdot (1 - \delta_{n,m}) \\ &+ \Re \left(i o^* \langle \chi_n | \left(\hat{H}_n^{c''} - i\delta t (\hat{H}_n^{c'})^2 \right) | \psi_n \rangle \right) \delta t \cdot \delta_{n,m}, \end{aligned} \quad (\text{A30})$$

Derivatives of the end points (corresponding to the outer 'rim' of the Hessian matrix) carry an additional factor 1/2 each, for a total of 1/4 in the corners and 1/2 on the edges. As with the gradient, the Hessian is similarly identical to (A21) when retaining only the $k = k_{\text{max}} = 0$ term. As an implementation detail, note that the propagated states and operator-state products from (12) may be re-used here. The second term is the most costly to evaluate because of additional state propagations. The order of evaluation should be row-by-row to further increase re-usability of computations.

b. Derivatives of $\hat{\mathcal{U}}_n^{\text{ST}_2}$

The Suzuki-Trotter expansion reads $\hat{\mathcal{U}}_n^{\text{ST}_2} = \hat{\mathcal{U}}_n^{c/2} \hat{\mathcal{U}}_n^d \hat{\mathcal{U}}_n^{c/2}$,

$$\frac{\partial J_F^{\text{ST}_2}}{\partial u_n} = -\Re \left(o^* \frac{\partial o}{\partial u_n} \right), \quad (\text{A31a})$$

$$\frac{\partial o}{\partial u_n} = \left\langle \chi_{n+1} \left| \frac{\partial \hat{\mathcal{U}}_n^{\text{ST}_2}}{\partial u_n} \right| \psi_n \right\rangle. \quad (\text{A31b})$$

Invoking Eq. (A14) for $\hat{\mathcal{U}}_n^{c/2}$ we find

$$\begin{aligned} \frac{\partial \hat{\mathcal{U}}_n^{\text{ST}_2}}{\partial u_n} &= \frac{\partial \hat{\mathcal{U}}_n^{c/2}}{\partial u_n} \hat{\mathcal{U}}_n^d \hat{\mathcal{U}}_n^{c/2} + \hat{\mathcal{U}}_n^{c/2} \hat{\mathcal{U}}_n^d \frac{\partial \hat{\mathcal{U}}_n^{c/2}}{\partial u_n} \\ &= -\frac{i\delta t}{2} \left(\hat{\mathcal{U}}_n^{c/2} \hat{H}_n^{c'} \hat{\mathcal{U}}_n^d \hat{\mathcal{U}}_n^{c/2} + \hat{\mathcal{U}}_n^{c/2} \hat{\mathcal{U}}_n^d \hat{\mathcal{U}}_n^{c/2} \hat{H}_n^{c'} \right) \\ &= -\frac{i\delta t}{2} \left(\hat{H}_n^{c'} \hat{\mathcal{U}}_n^{\text{ST}_2} + \hat{\mathcal{U}}_n^{\text{ST}_2} \hat{H}_n^{c'} \right) \end{aligned}$$

Here we also used that two diagonal matrices always commute, first to evaluate the recursive commutator $[\hat{H}_n^{c'}, \hat{H}_n^{c'}]_k = \hat{H}_n^{c'} \cdot \delta_{0,k}$ from (A14), and second to recombine the initial propagators since $[\hat{H}_n^{c'}, \hat{\mathcal{U}}_n^{c/2}] = 0$. Substituting back into Eqs. A31a-A31b we find

$$\begin{aligned} \frac{\partial o}{\partial u_n} &= -\frac{i\delta t}{2} \left\langle \chi_{n+1} \left| \left(\hat{H}_n^{c'} \hat{\mathcal{U}}_n^{\text{ST}_2} + \hat{\mathcal{U}}_n^{\text{ST}_2} \hat{H}_n^{c'} \right) \right| \psi_n \right\rangle \\ &= -\frac{i\delta t}{2} \left\{ \left\langle \chi_{n+1} \left| \hat{H}_n^{c'} \right| \psi_{n+1} \right\rangle + \left\langle \chi_n \left| \hat{H}_n^{c'} \right| \psi_n \right\rangle \right\} \\ &= -\frac{i\delta t}{2} \sum_{p=n}^{n+1} \left\langle \chi_p \left| \hat{H}_n^{c'} \right| \psi_p \right\rangle \end{aligned} \quad (\text{A32})$$

$$\Rightarrow \frac{\partial J_F^{\text{ST}_2}}{\partial u_n} = \Re \left(\frac{io^*}{2} \sum_{p=n}^{n+1} \left\langle \chi_p \left| \hat{H}_n^{c'} \right| \psi_p \right\rangle \right) \delta t, \quad (\text{A33})$$

for all $n = 1, \dots, N_t - 1$.

The Hessian elements are written as

$$\frac{\partial^2 J_F}{\partial u_n \partial u_m} = -\Re \left(\left(\frac{\partial o}{\partial u_m} \right)^* \frac{\partial o}{\partial u_n} + o^* \frac{\partial^2 o}{\partial u_n \partial u_m} \right). \quad (\text{A34})$$

and after some lines of calculation, the second derivatives of o evaluate to

$n > m :$

$$\begin{aligned} \frac{\partial^2 o}{\partial u_n \partial u_m} &= \\ &= -\frac{\delta t^2}{4} \sum_{p=n}^{n+1} \sum_{q=m}^{m+1} \left\langle \chi_p \left| \hat{H}_n^{c'} \left(\prod_{j=q}^{p-1} \hat{\mathcal{U}}_n^{\text{ST}_2} \right) \hat{H}_m^{c'} \right| \psi_q \right\rangle, \end{aligned} \quad (\text{A35a})$$

$n = m :$

$$\begin{aligned} \frac{\partial^2 o}{\partial u_n \partial u_m} &= -\frac{i\delta t}{2} \left(\sum_{j=n}^{n+1} \left\langle \chi_j \left| \left(\hat{H}_n^{c''} - \frac{i\delta t}{2} (\hat{H}_n^{c'})^2 \right) \right| \psi_j \right\rangle \right. \\ &\quad \left. - i\delta t \left\langle \chi_{n+1} \left| \hat{H}_n^{c'} \hat{\mathcal{U}}_n^{\text{ST}_2} \hat{H}_n^{c'} \right| \psi_n \right\rangle \right), \end{aligned} \quad (\text{A35b})$$

Substituting Eqs. A32,A35a,A35b into Eq. (A34) yields the final result,

$$\begin{aligned} \frac{\partial^2 J_F^{\text{ST}_2}}{\partial u_n \partial u_m} &= \Re \left\{ \right. \\ &+ \frac{1}{4} \sum_{p=n}^{n+1} \sum_{q=m}^{m+1} \left\langle \psi_q \left| \hat{H}_m^{c'} \right| \chi_q \right\rangle \left\langle \chi_p \left| \hat{H}_n^{c'} \right| \psi_p \right\rangle \delta t^2 \\ &+ \frac{o^*}{4} \sum_{p=n}^{n+1} \sum_{q=m}^{m+1} \left\langle \chi_p \left| \hat{H}_n^{c'} \prod_{j=q}^{p-1} \hat{\mathcal{U}}_n^{\text{ST}_2} \hat{H}_m^{c'} \right| \psi_q \right\rangle (1 - \delta_{n,m}) \delta t^2 \\ &+ \frac{io^*}{2} \left(\sum_{j=n}^{n+1} \left\langle \chi_j \left| \left(\hat{H}_n^{c''} - \frac{i\delta t}{2} (\hat{H}_n^{c'})^2 \right) \right| \psi_j \right\rangle \right. \\ &\quad \left. - i\delta t \left\langle \chi_{n+1} \left| \hat{H}_n^{c'} \hat{\mathcal{U}}_n^{\text{ST}_2} \hat{H}_n^{c'} \right| \psi_n \right\rangle \right) \delta_{n,m} \delta t \left. \right\}. \end{aligned} \quad (\text{A36})$$

Comparatively, the Hessian expression for $\hat{\mathcal{U}}_n^{\text{ST}_2}$ is are much more cumbersome than that for $\hat{\mathcal{U}}_n^{\text{ST}_1}$.

3. Derivatives for Regularizations

In many applications, it is advantageous to regularize either or both the control amplitude and its temporal derivative. This requires additional terms in the cost functional objective, imposing discretization, and calculating the respective derivatives. As with the propagator, the chosen form of the implementation scheme changes the derivative calculations.

The amplitude regularization is straightforward,

$$J_\alpha = \frac{\alpha}{2} \int_0^T u(t)^2 dt \rightarrow \frac{\alpha}{2} \delta t \sum_{i=1}^{N_t} u_i^2 \quad (\text{A37})$$

$$\frac{\partial J_\alpha}{\partial u_n} = \alpha \delta t u_n, \quad \frac{\partial^2 J_\alpha}{\partial u_m \partial u_n} = \alpha \delta t \delta_{n,m} \quad (\text{A38})$$

where α is a weighting factor. The derivative regularization is a bit more involved because of end points

$$\begin{aligned} J_\gamma &= \frac{\gamma}{2} \int_0^T \dot{u}(t)^2 dt \rightarrow \frac{\gamma}{8\delta t} \left(\sum_{i=2}^{N_t-1} (u_{i+1} - u_{i-1})^2 \right. \\ &\quad \left. [-3u_1 + 4u_2 - u_3]^2 + [3u_{N_t} - 4u_{N_t-1} + u_{N_t-2}]^2 \right) \end{aligned} \quad (\text{A39})$$

where we used forward (backward) difference approximations for the first (last) point and center approximations for the bulk, all to order $\mathcal{O}(\delta t^2)$. The derivative with respect to the first and last three indices is different from the bulk. The resulting gradient written in vector form

is

$$\nabla J_\gamma = \frac{\gamma}{4\delta t} \begin{bmatrix} 10u_1 - 12u_2 + 2u_3 \\ -12u_1 + 17u_2 - 4u_3 - u_4 \\ 2u_1 - 4u_2 + 3u_3 - u_5 \\ \vdots \\ 2u_n - u_{n-2} + u_{n+2} \\ \vdots \\ 2u_{N_t} - 4u_{N_t-1} + 3u_{N_t-2} - u_{N_t-4} \\ -12u_{N_t} + 17u_{N_t-1} - 4u_{N_t-2} - u_{N_t-3} \\ 10u_{N_t} - 12u_{N_t-1} + 2u_{N_t-2} \end{bmatrix}, \quad (\text{A40})$$

where the vertical dots extend over the bulk points. Similarly the three first and last Hessian rows are different from the bulk. In a stacking notation where the indices

denote the rows:

$$\nabla^2 J_\gamma = \begin{bmatrix} [\nabla^2 J_\gamma]_{1:3} \\ [\nabla^2 J_\gamma]_{4:N_t-3} \\ [\nabla^2 J_\gamma]_{N_t-2:N_t} \end{bmatrix} \quad (\text{A41})$$

where the matrices evaluate to

$$[\nabla^2 J_\gamma]_{1:3} = \frac{\gamma}{4\delta t} \begin{bmatrix} 10 & -12 & 2 & 0 & 0 & 0 & \dots \\ -12 & 17 & -4 & -1 & 0 & 0 & \dots \\ 2 & -4 & 3 & 0 & -1 & 0 & \dots \end{bmatrix}, \quad (\text{A42})$$

$$[\nabla^2 J_\gamma]_{4:N_t-3} = \frac{\gamma}{4\delta t} \begin{bmatrix} 0 & -1 & 0 & 2 & 0 & -1 & 0 & 0 & \dots \\ & \ddots & & \ddots & & \ddots & & & \\ \dots & 0 & 0 & -1 & 0 & 2 & 0 & -1 & 0 \end{bmatrix}, \quad (\text{A43})$$

$$[\nabla^2 J_\gamma]_{N_t-2:N_t} = \frac{\gamma}{4\delta t} \begin{bmatrix} \dots & 0 & -1 & 0 & 3 & -4 & 2 \\ \dots & 0 & 0 & -1 & -4 & 17 & -12 \\ \dots & 0 & 0 & 0 & 2 & -12 & 10 \end{bmatrix}, \quad (\text{A44})$$

where the dots denote continuation of the number they point to.

-
- [1] S. J. Glaser, U. Boscain, T. Calarco, C. P. Koch, W. Köckenberger, R. Kosloff, I. Kuprov, B. Luy, S. Schirmer, T. Schulte-Herbrüggen, *et al.*, The European Physical Journal D **69**, 279 (2015).
- [2] F. Motzoi, J. M. Gambetta, P. Rebentrost, and F. K. Wilhelm, Physical review letters **103**, 110501 (2009).
- [3] D. J. Egger and F. K. Wilhelm, Superconductor Science and Technology **27**, 014001 (2013).
- [4] M. H. Goerz, F. Motzoi, K. B. Whaley, and C. P. Koch, npj Quantum Information **3**, 1 (2017).
- [5] S. Montangero, *Introduction to Tensor Network Methods: Numerical simulations of low-dimensional many-body quantum systems* (Springer International Publishing, 2018).
- [6] M. Dalgaard, F. Motzoi, J. J. Sørensen, and J. Sherson, npj Quantum Information **6**, 6 (2020).
- [7] C. T. Kehlet, A. C. Sivertsen, M. Bjerring, T. O. Reiss, N. Khaneja, S. J. Glaser, and N. C. Nielsen, Journal of the American Chemical Society **126**, 10202 (2004).
- [8] N. Khaneja, T. Reiss, C. Kehlet, T. Schulte-Herbrüggen, and S. J. Glaser, Journal of magnetic resonance **172**, 296 (2005).
- [9] N. C. Nielsen, C. Kehlet, S. J. Glaser, and N. Khaneja, eMagRes (2007).
- [10] W. Kallies and S. J. Glaser, Journal of Magnetic Resonance **286**, 115 (2018).
- [11] J. J. Sørensen, J. S. Nyemann, F. Motzoi, J. Sherson, and T. Vosegaard, The Journal of Chemical Physics **152**, 054104 (2020).
- [12] J. Scheuer, X. Kong, R. S. Said, J. Chen, A. Kurz, L. Marseglia, J. Du, P. R. Hemmer, S. Montangero, T. Calarco, *et al.*, New Journal of Physics **16**, 093022 (2014).
- [13] F. Dolde, V. Bergholm, Y. Wang, I. Jakobi, B. Naydenov, S. Pezzagna, J. Meijer, F. Jelezko, P. Neumann, T. Schulte-Herbrüggen, *et al.*, Nature communications **5**, 1 (2014).
- [14] G. Waldherr, Y. Wang, S. Zaiser, M. Jamali, T. Schulte-Herbrüggen, H. Abe, T. Ohshima, J. Isoya, J. Du, P. Neumann, *et al.*, Nature **506**, 204 (2014).
- [15] Y. Chou, S.-Y. Huang, and H.-S. Goan, Physical Review A **91**, 052315 (2015).
- [16] C. P. Koch, J. P. Palao, R. Kosloff, and F. Masnou-Seeuws, Physical Review A **70**, 013402 (2004).
- [17] C. P. Koch, E. Luc-Koenig, and F. Masnou-Seeuws, Physical Review A **73**, 033408 (2006).
- [18] E. F. De Lima, T.-S. Ho, and H. Rabitz, Chemical Physics Letters **501**, 267 (2011).
- [19] K. M. Tibbetts, X. Xing, and H. Rabitz, Physical Chemistry Chemical Physics **15**, 18012 (2013).
- [20] P. Doria, T. Calarco, and S. Montangero, Physical review letters **106**, 190501 (2011).
- [21] S. van Frank, M. Bonneau, J. Schmiedmayer, S. Hild, C. Gross, M. Cheneau, I. Bloch, T. Pichler, A. Negretti, T. Calarco, and S. Montangero, Scientific Reports **6**, 34187 (2016).
- [22] M. Mundt and D. J. Tannor, New Journal of Physics **11**, 105038 (2009).
- [23] G. Jäger and U. Hohenester, Physical Review A **88**, 035601 (2013).
- [24] J. Cui, R. van Bijnen, T. Pohl, S. Montangero, and T. Calarco, Quantum Science and Technology **2**, 035006 (2016).

- (2017).
- [25] S. Patsch, D. M. Reich, J.-M. Raimond, M. Brune, S. Gleyzes, and C. P. Koch, *Physical Review A* **97**, 053418 (2018).
 - [26] P. De Fouquieres, S. Schirmer, S. Glaser, and I. Kuprov, *Journal of Magnetic Resonance* **212**, 412 (2011).
 - [27] S. Machnes, U. Sander, S. Glaser, P. de Fouquieres, A. Gruslys, S. Schirmer, and T. Schulte-Herbrüggen, *Physical Review A* **84**, 022305 (2011).
 - [28] S. Machnes, D. J. Tannor, F. K. Wilhelm, and E. Assémat, *arXiv:1507.04261* (2015).
 - [29] J. Sørensen, M. Aranburu, T. Heinzel, and J. Sherson, *Physical Review A* **98**, 022119 (2018).
 - [30] D. J. Tannor, V. Kazakov, and V. Orlov, in *Time-dependent quantum molecular dynamics* (Springer, 1992) pp. 347–360.
 - [31] J. P. Palao and R. Kosloff, *Physical review letters* **89**, 188301 (2002).
 - [32] S. G. Schirmer and P. de Fouquieres, *New Journal of Physics* **13**, 073029 (2011).
 - [33] T. Caneva, T. Calarco, and S. Montangero, *Physical Review A* **84**, 022326 (2011).
 - [34] D. Sels, *Physical Review A* **97**, 040302 (2018).
 - [35] X. Li, D. Pecak, T. Sowiński, J. Sherson, and A. E. Nielsen, *Physical Review A* **97**, 033602 (2018).
 - [36] J. J. Sørensen, M. Aranburu, T. Heinzel, and J. Sherson, *arXiv:1802.07521* (2018).
 - [37] D. Dong and I. R. Petersen, *IET Control Theory & Applications* **4**, 2651 (2010).
 - [38] F. Caruso, S. Montangero, T. Calarco, S. F. Huelga, and M. B. Plenio, *Physical Review A* **85**, 042331 (2012).
 - [39] I. Walmsley and H. Rabitz, *Physics Today* **56**, 43 (2003).
 - [40] S. Rosi, A. Bernard, N. Fabbri, L. Fallani, C. Fort, M. Inguscio, T. Calarco, and S. Montangero, *Physical Review A* **88**, 021601 (2013).
 - [41] G. Feng, F. H. Cho, H. Katiyar, J. Li, D. Lu, J. Baugh, and R. Laflamme, *Physical Review A* **98**, 052341 (2018).
 - [42] R. Heck, O. Vuculescu, J. J. Sørensen, J. Zoller, M. G. Andreassen, M. G. Bason, P. Ejlertsen, O. Elíasson, P. Haikka, J. S. Laustsen, L. L. Nielsen, A. Mao, R. Müller, M. Napolitano, M. K. Pedersen, A. R. Thorsen, C. Bergenholtz, T. Calarco, S. Montangero, and J. F. Sherson, *Proceedings of the National Academy of Sciences* **115**, E11231 (2018), <https://www.pnas.org/content/115/48/E11231.full.pdf>.
 - [43] J. H. M. Jensen, M. Gajdacz, S. Z. Ahmed, J. H. Czarkowski, C. Weidner, J. Rafner, J. J. Sørensen, K. Mølmer, and J. F. Sherson, *arXiv:2004.03296* (2020).
 - [44] A. Acín, I. Bloch, H. Buhrman, T. Calarco, C. Eichler, J. Eisert, D. Esteve, N. Gisin, S. J. Glaser, F. Jelezko, *et al.*, *New Journal of Physics* **20**, 080201 (2018).
 - [45] J. Nocedal and S. J. Wright, *Numerical optimization 2nd* (Springer Science & Business Media, New York, 2006).
 - [46] D. Goodwin and I. Kuprov, *The Journal of chemical physics* **143**, 084113 (2015).
 - [47] D. Goodwin and I. Kuprov, *The Journal of chemical physics* **144**, 204107 (2016).
 - [48] H. Hogben, M. Krzystyniak, G. Charnock, P. Hore, and I. Kuprov, *Journal of Magnetic Resonance* **208**, 179 (2011).
 - [49] Assuming the control Hamiltonians commute such as to be simultaneously diagonalizable, otherwise the following situation becomes a bit more complicated and requires further, similar analysis.
 - [50] A. Borzi, G. Ciaramella, and M. Sprengel, *Computational Science & Engineering* (Society for Industrial and Applied Mathematics, 2017) p. 397.
 - [51] U. Schollwöck, *Annals of Physics* **326**, 96 (2011).
 - [52] G. C. Hegerfeldt, *Physical review letters* **111**, 260501 (2013).
 - [53] G. E. Santoro, R. Martoňák, E. Tosatti, and R. Car, *Science* **295**, 2427 (2002).
 - [54] T. Caneva, T. Calarco, R. Fazio, G. E. Santoro, and S. Montangero, *Physical Review A* **84**, 012312 (2011).
 - [55] T. Caneva, M. Murphy, T. Calarco, R. Fazio, S. Montangero, V. Giovannetti, and G. E. Santoro, *Physical review letters* **103**, 240501 (2009).
 - [56] M. Dalgaard, F. Motzoi, J. H. M. Jensen, and J. Sherson, *arXiv:2006.00935* (2020).
 - [57] J. H. M. Jensen, F. S. Møller, J. J. Sørensen, and J. F. Sherson, *arXiv:2008.06076* (2020).
 - [58] T. J. Park and J. Light, *The Journal of chemical physics* **85**, 5870 (1986).
 - [59] M. Hochbruck and C. Lubich, *SIAM Journal on Numerical Analysis* **34**, 1911 (1997).
 - [60] R. Beerwerth and H. Bauke, *Computer Physics Communications* **188**, 189 (2015).
 - [61] M. L. Boas, *Mathematical methods in the physical sciences* (John Wiley & Sons, 2006).
 - [62] J. J. Sakurai and E. D. Commins, “Modern quantum mechanics, revised edition,” (1995).